Chapter 8

Image-Guided Hypofractionated Radiosurgery of Large and Complex Brain Lesions

Dilini Pinnaduwage, Peng Dong and Lijun Ma

Additional information is available at the end of the chapter

http://dx.doi.org/10.5772/64481

Abstract

Hypofractionated radiosurgery either through frame or image guidance has emerged as the most important area of research and development for intracranial and extracranial radiosurgery. In this chapter, we focused on discussions of three state-of-the-art platforms: Frame- and Image-Guided Gamma Knife, Robotic X-Band Cykerknife, and Flattening-Filter-Free intensity-modulated S-band medical linear accelerators. Practical principles with detailed workflow and clinical implementations are presented in a systematic approach. With rapid evolvement of both hardware and software in the realm of delivering hypofractionated radiosurgery, this chapter aims to offer a reader physical clarity on judging and balancing of achieving high-precision and high-quality treatments with practical examples and guidelines on intracranial applications.

Keywords: hypofractionation, radiosurgery, Gamma Knife, Cyberknife, flattening filter free, linear accelerator

1. Hypofractionated Gamma Knife radiosurgery

The genesis of radiosurgery dated to the late 1940s when Swedish neurosurgeon Professor Dr. Lars Leksell pioneered the first stereotactic radiosurgery (SRS) device called Gamma Knife. The basic concept of radiosurgery (e.g., performing surgery without a scapel but with invisible photon rays) was revolutionary at the time, and it took several trials for Leksell to convince his peers and published his first paper on the device [1].

A key turning point in worldwide utilization of Gamma Knife radiosurgery (GKSRS) was its first North American installation at the University of Pittsburgh in 1987 [2]. Gradually and steadily, GKSRS has been demonstrated to be a highly successful modality in managing many

benign and malignant indications [3–9]. However, due to the finite beam collimation size (maximum beam collimator diameter of 1.6–1.8 cm) and manual setups of individual patients, majority of the targets treated are relatively small lesions (e.g., <4 or 5 cm in maximum target dimension) and are generally treated in a single fraction [6, 9].

In 2006, GKSRS system underwent a redesign from ground up and the Leksell Gamma Knife Perfexion (PFX) was introduced in 2006, first in France, the UK, and then in the USA [10–13]. The key features of the PFX included an automatic submillimeter patient-positioning couch and a universal collimator system automatically aligns the radiation beamlets for variable collimation sizes. These new improvements physically eliminated manual setups of the early GKSRS models. As a result, GKSRS treatment delivery has become a turnkey solution and a large number of isocenters to be readily delivered with the minimum treatment effort. This greatly expanded the traditional GKSRS capability of treating large targets with a high number of isocenters.

With the advent of imaging guidance, the most recently developed Leksell Gamma Knife Icon (LGKI) has enabled repeatable patient setups without an invasive immobilization of an invasive metal frame, thus ushered in a new era of delivering hypofractionated GKSRS without number of isocenter restrictions. The general practice principles of GKSRS and its associated technical features of LGKI are described in detail in this section.

1.1. General physical principles

Unlike traditional C-arm radiation therapy delivery where a single source of radiation is employed and the radiation beams are delivered one beam after another in a sequential manner, GKSRS was designed from the start to employ hundreds of radiation beams to cross-fire in a simultaneous manner. In general, radiosurgical treatment delivery can be classified into four-type treatment delivery paradigms: (1) immobilize patient and radiation beams together, (2) mobilize patient and radiation beams together, (3) immobilize patient but mobilize radiation beams, and (4) mobilize patient but immobilize radiation beams.

The first and second types of treatment delivery are uncommon and employed primarily in specialized treatments such as ocular melanoma treatment, etc. Most of modern linac-based radiosurgical treatments employed the third type of delivery, where the patient or the treatment target was typically immobilized through various means, and radiation beams are delivered in sequence with the general assumption that patient's or target's position remained unchanged during the beam irradiation.

In contrast, GKSRS is a classic example of employing the fourth type of delivery, that is, all the radiation beams were fixed and the patient's positioning are adjusted from time to time to allow radiation dose delivered to different spots inside a 3D target volume. As a result, the overall precision involved in the treatment for GKSRS is largely governed by the positioning accuracy of the patient itself. The latest GKSRS PFX and Icon device have further improved general accuracy of GKSRS by employing fully digitally controlled patient positioning system (PPS) and patient surveillance system (PSS). With frame-based as well as latest infrared

http://dx.doi.org/10.5772/64481

marker-based patient positioning monitoring capability, the system has been updated to detect mechanical shifts in the range of a few microns.

Figure 1 shows the latest GKSRS device, that is, the PFX and LGKI unit. Unlike previous GKSRS models, both PFX and LGKI employ a combination of the third and the fourth delivery paradigm as discussed above to achieve unmatched dose painting in the treatment planning process (the details of such a capability are described in the following section). In another word, once the patient is immobilized and aligned based on a pre-prescribed fixed position, the radiation beams become changeable while the patient is in position through a unique universal collimator system and a fully automatic couch patient positioning system as shown in the panel (a) of **Figure 1**. The details of the system components of the PFX and LGKI for hypofractionated GKSRS are described in the following paragraphs.

Figure 1. (a) The Leksell Gamma Knife Perfexion (PFX) units and (b) Lekesell Gamma Knife Icon (LGKI) unit. Both systems possessed the same radiation generation mechanism through 192 Co-60 beams and a tungsten universal collimator behind a shield door as shown in Panel (a). The key difference between the two systems is the addition of a stereostatic cone-beam CT arm mounted for the LGKI unit as shown in Panel (b).

In summary, current GKSRS delivery through either PFX or LGI has enabled a combination of treatment delivery paradigms that successfully integrated mechanisms of precision patient immobilization (either with relocatable frame of PFX or with imaging-guided masking system of LGI) and the precision radiation beam alignment techniques to deliver adaptive hypofractional radiosurgical treatments. In the words of the Professor Dr. Lars Leksell, inventor of Gamma Knife: "The tools used by the surgeons must be adapted to the task and where the human brain is concerned they cannot be too refined". This is certainly the case for hypofractionated brain radiosurgery.

1.2. System design, hardware and work flow

One of the hallmarks of GKSRS was its Leksell G-frame system for immobilization of the skull of a patient. Besides being sturdy in securing and immobilizing the patient's skull for beam referencing, a major physical advantage of the frame is its elimination of rotational shifts required in patient setups. In another word, any point in the space can be readily reached with simple translational shifts along *x*-, *y*-, and *z*-directions once the frame has established its Cartesian coordinate system. However, due to invasive nature of the frame and current

medical reimbursement rules in the USA, the frame-based GKSRS treatment was primarily limited to the single fraction GKSRS.

Recognizing the restrictions with the metal frame for delivering hypofractionated treatments, a vacuum-assisted relocatable frame system, that is, GK eXtend [14–17] was introduced shortly after the introduction of the PFX system in 2006. **Figure 2** illustrated the construction of such a relocatable frame system in actual clinical practice.

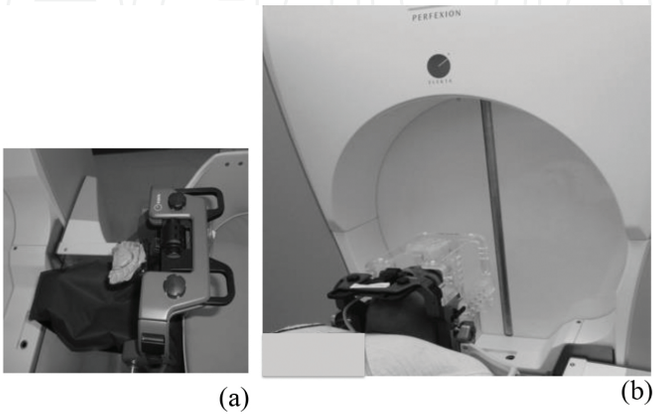

Figure 2. Illustration of the GKSRS relocatable eXtend frame system shows: (a) the components of the customized eXtend frame with bite-block molded and docked onto the PFX unit and (b) the actual patient using the eXtend frame prior to the treatment delivery.

The relocatable frame as shown in the figure was adapted and improved over the conventional radiation therapy bite-block immobilization device. One major improvement is the use of vacuum assistance and saliva control cups that allow the bite-block to be anchored unto the hard palate in the patient's mouth. Together with vacuum cushion of the headrest (**Figure 3a**) supporting the back of the patient's skull, the patient's head immobilized with respect to the two lateral posts that is attached to the couch.

Evidently, the accuracy of such a relocatable frame depends on the positioning repeatability of the patient. **Figure 3b** shows the plastic template box attached to the superior of the patient head for such a purpose. The plastic template box was used to check the repeatability of the frame setup through the traditional dip-stick measurements, where the skull surface of variable points was measured before the treatment to ensure correct frame setups. In the case of eXtend frame showing in **Figure 3b**, such measurements were manually conducted through a calibrated digital probe, and measurement results were compared with the reference values taken at the time of the patient's CT scanning. An illustration of the probe measurement in conjunction with the patient setup of **Figure 2** is shown in **Figure 4**.

Several studies utilizing the PFX eXtend system have reported in-phantom as well as in-patient accuracy of 1 mm or less [16, 17]. One study primarily investigated the whole-procedural accuracy of the hypofractionated GKSRS treatments through the generalized end-to-end Winston-Lutz measurements as well as intrafractional patient data analysis [16]. The 3D radiological setup accuracy was determined to be 0.69 ± 0.73 mm (1σ) from a series of n = 58

http://dx.doi.org/10.5772/64481

treatment session, and the mean 90% confidence level range of uncertainties was found to be 0.55, 0.78, and 0.72 mm along the *x*-, *y*-, and *z*-axis, respectively.

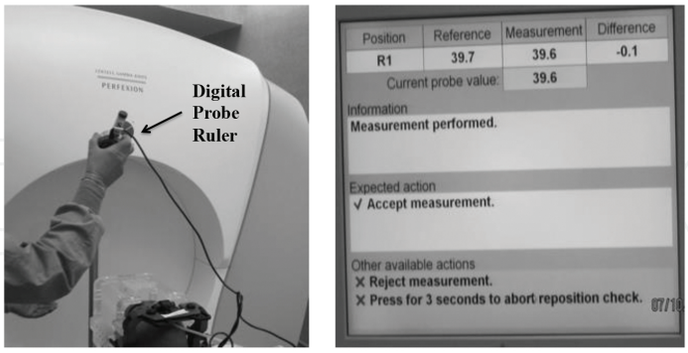

Figure 3. Illustration of the digital probe measurements for the hypofractionated GKSRS setups with the relocatable eXtend frame system on the PFX unit shows: (a) the hand-held digital probe ruler with the actual patient setups and (b) the measurement result of the probe at one template position. The difference displayed between the reference measurement and the actual measurement in (b) was in the unit of millimeter.

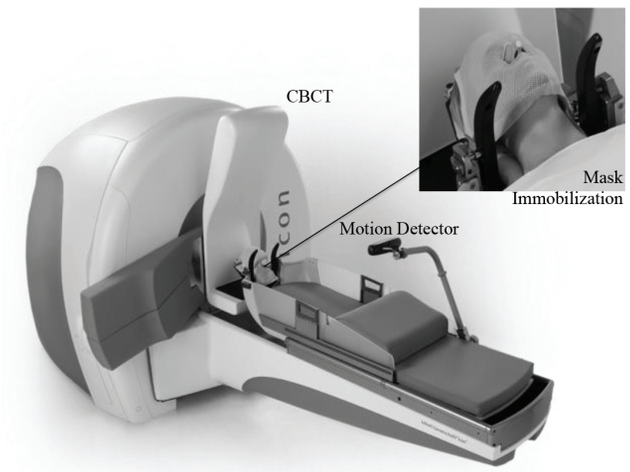

Figure 4. Major add-on system components of the Gamam Knife Icon (GKI) compared to the PFX include (1) a patient masking immobilization system (upper insert); (2) an on-line 3D imaging capability with stereotactic calibrated cone-beam CT device; and (3) a high-definition patient motion monitoring detector and feedback control system.

Evidently, the whole-procedural accuracy of these measurements included the positioning accuracy by the full couch motions. Given that multiple shots are typically used for hypofractionated treatments of relatively large lesions, the wear-and-tear of the couch in performing thousands of the patient setups may become a concern to ensure submillimeter accuracy. To investigate such problem, the central positioning as well as off-center couch positioning consistency was investigated through the so-called "picket fence" testing for a high-volume treatment center [18]. The study found an overall accuracy consistency of 0.03 ± 0.24 (2σ) mm. Such a value matched excellently with the manufacturer's mechanical specification of 0.35 mm

even after repeated use of completing >1000 treatment cases. Based on the results of the study, the overall 3D vector accuracy was predominantly contributed by patient-specific rather than hardware-related in hypofractionated GKSRS treatments with the relocatable eXtend frame system.

Of note, patients to be treated with eXtend frame system need to be carefully selected before applying the relocatable eXtend frame system, specifically in regard to the performance status, gum health, and teeth integrity. With a team of experienced radiation therapy, users familiar with fabrication of conventional radiation therapy bite-blocks and managing patient's oral hygiene, hypofractionated GKSRS treatment with the PFX eXtend frame was an excellent option for expanding the traditional single-fractional GKSRS program.

Nearly a decade from the initial introduction of GK PFX system in 2006, US Food and Drug Administration and Nuclear Regulatory Commission have recently approved the image-guided Gamma Knife Icon (GKI) system. The GKI system is an integration of the PFX system with a 3D CBCT and a high-definition patient motion management system as shown in **Figure 5**. The 3D CBCT was designed to correct both translational and rotational shifts encountered during the initial patient setups when immobilized with the mask system. The patient motion management system monitors the patient's head positioning during the treatment delivery through a reflective marker placed on the patient's nose bridge in reference to the two lateral black post points as shown in the insert of **Figure 5**.

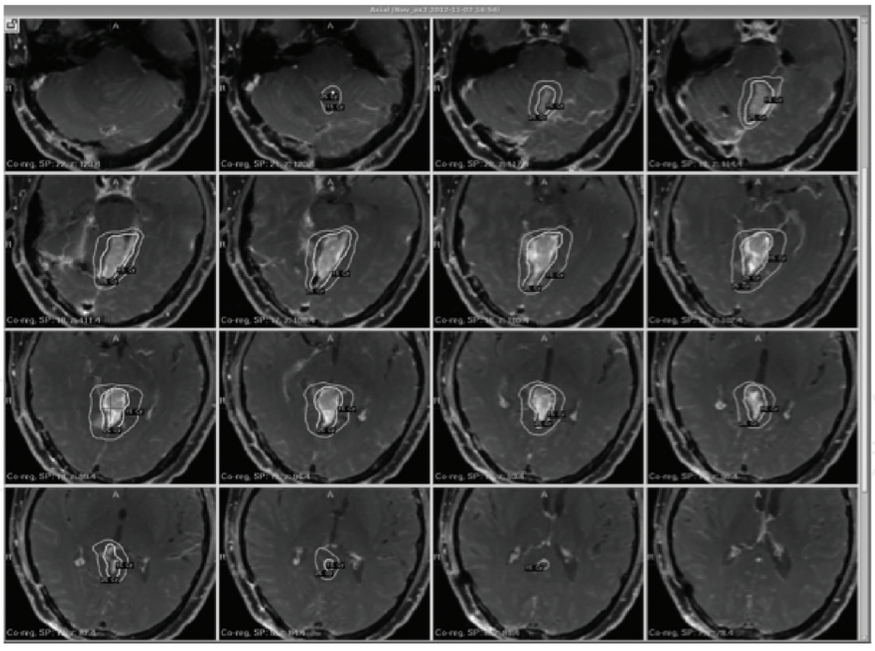

Figure 5. Axial dose distributions of a hypofractionated GKSRS treatment as planned with Leksell Gamma Plan (LGP version 10.2) for PFX or GKI treatments. Note the sharp dose fall-off along the posterior portion of the brainstem for maximum dose sparing.

The hypofractionated GKSRS workflow is similar among the eXtend frame system and the mask-based GKI system, where patient will undergo traditional MR and CT scans before the

http://dx.doi.org/10.5772/64481

treatment. However, the available of online 3D imaging guidance as offered by the GKI system allows the patient to be scanned without a tertiary frame, thus artifacts or susceptibility uncertainties introduced by these devices are eliminated from the workflow. In essence, on-device 3D CBCT serves not only as a "virtual" stereotactic frame but also as on-treatment patient positioning detection system.

Another important feature of GKI is its online dose recalculation and/or dose adaption workflow based on the 3D positioning as detected in vivo. In another word, once the patient position is measured by the CBCT, the 3D dose distribution based on the live patient setups (i.e., target location) will be recalculated and reference to the original treatment planning generated dose distributions. The attending physician and authorized medical physicist (AMP) for the treatment are afforded the opportunity to review or revise and approve the treatment plan before initiation of actual treatment delivery. The unique dose sculpting capability of the Leksell Gamma Plan (LGP) allows such a process to be an efficient and robust procedure.

1.3. Treatment planning and dosimetric evaluation

Compared to the early GKSRS treatment delivery, a user quickly would notice a major paradigm shift in planning PFX or GKI-based treatment delivery versus the previous Gamma Knife models. Traditionally, each isocenter or called a "shot" in the GKSRS is set and verified either manually or semi-manually through a tertiary add-on manipulator. As a result, using fewer numbers of shots to accomplish a treatment plan is desirable to ensure treatment delivery efficiency and patient comfort. Therefore, a user tends to optimize a treatment plan with mindset of minimizing the total number of shots as much as possible.

With the automatic full couch positioning system as in PFX or GKI, delivering multiple shots has become a turnkey solution. This has significantly shifted treatment-planning practices and in essence rendered hypofractionated treatment of relatively large or complex lesions a logical fit for planning with the PFX or GKI system. Without repeating many excellent reviews on classical GKSRS treatment planning techniques, we here focus on specific issues related to the hypofractionted treatment planning.

Figure 6 illustrated a 3D axial isodose distribution of a large hypofractionated GKSRS meningioma case, where 25 Gy in five fractions were prescribed to 50% of the maximum dose inside the target. Note the significant sharper dose fall-off along the brainstem surface area for the lesion as created by the planner when applying a relatively high number of shots (n = 28) and liberal use of the smallest collimator shots (i.e., 4 mm in nominal beam diameter) along the brainstem surface area.

Since single-session dose of 5 Gy is significantly lower than the traditional GKSRS of 15–20 Gy per session, the total number of shots can be used is therefore largely constrained by the minimum amount of radiation that can be delivered per shot. For example, if the maximum dose rate for the given treatment session is 3 Gy per minute, then 0.3 Gy would be minimum dose required per shot within the mechanical timer accuracy of 0.1 min per shot. As a result, the contribution from each shot should be at least 0.3 Gy for this case, thus limiting the total

number of shots may be used for delivering such a treatment. This is a unique phenomenon for hypofractionated GKSRS.

Figure 6. The Cyberknife VSI system installed in a clinical setting. Note the two X-ray tubes mounted on the ceiling and the X-ray detectors that are placed beneath the floor of the treatment vault for stereotactic imaging and on-line tracking.

Evaluation of hypofractionated GKSRS treatment plans as illustrated in **Figure 6** is identical to the conventional GKSR, that is, dosimetric treatment planning indices such as Paddick conformity index (PCI) [19] and gradient index (GI) [20] similarly apply to single as well as hypofractionated GKSRS.

In summary, the PCI is defined as PCI = $(TIV)^2/(PIV \times TV)$, where TIV is the volume of the target falls inside 100% of the prescription isodose surface, PIV is the total 100% prescription isodose volume, and TV is the total target volume. In parallel, the GI is defined as GI = PIV50/PIV, where PIV50 is the total isodose volume enclosed by 50% of the prescription dose.

From the definitions of PCI and GI of the above, PCI is a direct measurement of how well the prescription isodose volume match or "conform" to the target volume, and GI is the measure of how steep the planned dose distribution falls beyond the prescription isodose surface. Studies have been carried out to investigate the best possible dose gradient that can be achieved for general GKSRS, and an empirical power law was found to describe such a dose fall-off near perfectly yielding high linear correlation of > 90% [12, 21].

In the context of hypofractionated treatment delivery, it is worth noting that PIV50 can be easily replaced with PIV30, PIV40, PIV60, etc. (e.g., 30, 40, 60, etc.) prescription isodose volumes to expand the definition of GI and allow detailed survey of the isodose dose effects associated with hypofractionated treatments. Unlike single fractional GKSRS delivery where peripheral isodose volumes around PIV50 such as the 10-Gy or 12-Gy isodose volumes have been reported

http://dx.doi.org/10.5772/64481

to surrogated the treatment complications such as symptomatic radiation necrosis rate, relevant isodose volumes for variable fractionation schemes such as 3–5 fractions have yet been established. Therefore, a user need to be careful in examining the peripheral isodose fall-off measures such as the PIV30, PIV40 or PIV60, etc. for all treatments until future clinical data and guidelines become available.

1.4. Future direction and developments

With the advent of GKI, hypofractionated GKSRS treatments expected to expand rapidly in the years ahead. Initial studies have shown excellent precision as well as robustness for patient positioning correction capability that rival frame-based treatment deliveries. With reduced dose for each hypofractionated treatment session such as 5–8 Gy and integrated stereo-CBCT treatment setups with direct coordinates adaption, the overall treatment delivery time with GKI would be expected to be 30 min or less that making it match well with other treatment modalities.

Several studies have indicated superior dose sculpting capabilities of PFX and GKI versus early GK SRS models [11]. Further treatment planning studies have also suggested equivalency of linac-based delivery with an early GK model [22]. Such a result supports the general finding of superiority of PFX and GI versus the linac-based treatment in sparing normal brain tissues [23–25]. These studies have clearly fortified the leading role of GKSRS in performing intracranial hypofractionated SRS.

However, it is worth mentioning several ongoing efforts in continually improving the dosimetric capabilities of GKSRS. One study has proposed the notion of dynamic GKSR delivery, where the whole treatment can be delivered through single path motion (i.e., the beam is always on during a treatment) in contrast to the step-and-shoot type of delivery [26]. One major improvement in the dosimetric properties noted was the significant improvements in the dose homogeneity within the target as well as some improvements in the peripheral dose fall-off, a likely contribution from the increased number of the beams associated with the treatment delivery.

Another study leveraging the power of sector beam mixing has proposed the concept of simultaneous intensity modulation for GKSRS [27]. In the mode of such a delivery, the intensity levels in 2π arrangement become fully variable from either zero (closed sector beam) to unity (open sector beam) during each shot delivery. It was found that significant normal tissue sparing improvements achieved by adding the sector intensity modulation for complex treatment cases such as epilepsy and for large lesion treatments involving a high number of isocenters. The latter of which is clearly relevant for the hypofractionated GKSRS. One key advantage noted with sector-beam intensity modulation is that the total beam-on time is equivalent to the traditional nonmodulated treatment deliveries thus making the approach clinically ready with the current PFX and GKI hardware design. Ongoing and further studies will determine whether dosimetric improvements as discussed above would translate into clear clinical advantages, especially in the developments of hypofractionated GKSRS.

2. Hypofractionated robotic CyberKnife radiosurgery

The CyberKnife (CK) is an image-guided, frameless, robotic radiosurgery system invented by John Adler and his team in the late 1980s [28, 29]. Unlike in the Gamma Knife system where Gamma rays from Co-60 decay are used for treatments, the CyberKnife system uses X-rays generated from a linear accelerator for radiation treatments. While the system received FDA clearance to treat head and neck, and upper spine lesions in 1999, in 2001, clearance was given to treat lesions located anywhere in the body. Therefore, the current system can be used for both intracranial and extracranial (spine, lung, liver, pelvis, etc.) radiation treatments. The CK system is not only an integrated unit consisting of treatment planning, imaging, and delivery, but also unique in its ability to continuously track, detect, and correct for both tumor and patient motion during treatment.

2.1. System descriptions and working principle

CyberKnife treatments are delivered through a motorized robotic manipulator (KUKA robot) that is attached to a lightweight X-band linear accelerator (linac) (**Figure 3**). The robotic manipulator allows for six degrees of freedom in positioning the radiation source, and allows for noncoplanar, nonisocentric beam delivery. The linac generates 6 MV photons, at a nominal dose rate of up to 1000 cGy/min. The manipulator is programmed to move within a fixed, predetermined workspace, and positions the radiation source at pre-assigned points within this workspace referred to as "nodes". At each node, the linac can deliver radiation from multiple beam angles [30]. Dose is delivered from "paths," which comprise of a series of nodes, determined during treatment planning. During treatment delivery, the manipulator moves the accelerator from node to node in sequence and delivers dose at those nodes selected during planning. The treatment path adopted by the robotic manipulator is dependent on the target location and patient anatomy as specified during treatment planning.

The radiation is collimated using either 12 interchangeable tungsten cones (known as "fixed" collimators), or the Iris™ (a variable aperture collimator [31]), both with aperture diameters ranging from 5 to 60 mm at a SAD of 800 mm. The Iris™ is made of two offset banks of six tungsten segments each, which combine to create dodecahedral apertures. With the Iris, the robot traverses the treatment path only once while delivering radiation from multiple collimating apertures at the chosen node position. In comparison, with the CK fixed cone system, the robot has to traverse the treatment path separately for each fixed cone size used for the treatment. Therefore, the Iris allows the use of multiple collimating apertures for a given treatment without drastically increasing treatment time. The newly released CK M6 platform, available for clinical use today, is additionally equipped with a multi leaf collimating (MLC) system that provides further potential for improved efficiency in the treatment delivery. This MLC system (CK InCise MLC system, Accuray Inc.) consists of 41 tungsten leaf pairs of 90 mm height and 2.5mm thickness at 800 mm SAD, and allows for a maximum field size of 120 (in the leaf motion direction) × 100 mm at 800 mm SAD. Leaf motion allows for 100% over-travel and full leaf inter-digitation, and has an average (intra-leaf, inter-leaf, and leaf tip) transmission of <0.3% [32].

http://dx.doi.org/10.5772/64481

The tracking volume (or the target volume itself) is stereotactically localized using orthogonal kV X-ray images. X-rays in the diagnostic energy range are generated from two X-ray sources that are attached to the treatment room ceiling. The X-rays exiting the patient are detected by amorphous silicon flat panel detectors, which are embedded beneath the floor. The imaging center, or the point in space at which these imaging beams intersect, is referred to as the "align center". The geometry of the imaging system is such that the patient is imaged at a 45° angle. The high-resolution digital X-ray images obtained during patient setup and treatment are automatically registered to a set of digitally reconstructed radiographs (DRRs) generated from the treatment planning CT. The difference in patient positioning from simulation to treatment in the three translation and rotational directions are calculated based on this 2D–2D registration. During treatment, the patient is imaged at an imaging frequency that can be specified by the operator. The imaging frequency can be set between 15 and 150 sec, and it is common to image the patient at time intervals of 30–60 sec in the case of brain treatments. During treatment delivery, the robotic manipulator compensates for the differences seen in the patient, or target position, by redirecting the radiation beam to the actual target position in near-real time.

2.2. Treatment simulation and inverse planning

Proper patient simulation is critical to ensure an accurate treatment delivery. While it is imperative in radiation therapy in general, to achieve a patient setup that is both easily reproducible and comfortable for the patient, for CK treatments the patient setup should in addition adhere to specific patient safety zone requirements. The CK system consists of two virtual safety zones, named the "fixed safety zone" and the "dynamic safety zone". These safety zones are designed as safety mechanisms to prevent robot collisions with the patient. The fixed safety zone is based on the imaging center and varies in dimension depending on the treatment site (i.e., head vs. body). The dynamic safety zone is located within the fixed safety zone [30, 33]. It includes all of the patient body and varies in size based on the individual patient's size (small, medium, and large) as specified by the therapist.

For brain treatments, custom-made head masks are used to immobilize the patient. An appropriate headrest is chosen so that the patient's neck is in a comfortable position. In particular, hyperextended or flexed neck positions are discouraged, as treatment times can be as long as 30 min for a typical brain treatment. The treatment times could be even longer for multiple brain metastasis treatments, based on the number of lesions, lesion size, and prescription dose to each. The patient's arms and knees should be placed in compliance with the patient safety zone requirements discussed above.

CT simulation is performed with the patient in the supine position. A contiguous, no gap CT scan is obtained with a 1–1.5 mm slice thickness. The slice thickness is important as thinner slices generate better quality DRRs improving the tracking accuracy [34]. The CT field-of-view should be reasonable (typically 30 cm) and not unnecessarily large for improved image quality. The scan should be centered on the target and includes the entire patient head as the tracking algorithm for brain treatments is based on the patient's skull features. The primary CT used for treatment planning should be a noncontrast CT as contrast in the scan may impact dose

calculation and tracking accuracy. If a contrast CT is needed, the contrast CT can be imported into the planning system as a secondary image set.

2.2.1. Image registration and structure contouring

For brain CK treatments, MR imaging is used for target delineation because MR provides better soft tissue visualization compared to CT. Certain critical structures such as the brainstem and chiasm are also better visualized on MR. Because dose calculation for treatment planning is based on CT, the MR images are imported into the planning system as secondary image set and coregistered with the primary CT data set. Several image registration options are available within the CK treatment planning software. For most brain cases, the automatic registration feature is commonly used, and the user can specify the region of interest for the auto-registration. This algorithm uses intensity values based on mutual information. In addition, a semiautomatic point based, and manual registration methods are also available. Once target contouring is complete, critical structures are delineated. MR images are then used to define certain critical structures such as the brainstem and chiasm, whereas the some other structures such as the optic nerves and cochlea can be better defined based on the planning CT.

The difficulty level of treatment planning for brain lesions can vary depending on the target location and proximity to critical structures such as the brain stem and optic structures. For those cases in which the critical structures are in close proximity to the target volume, planning risk volumes (PRVs) may be generated by expanding those critical structures by ~2–3 mm and by ensuring that these PRV volumes are well within their dose tolerance during the treatment planning process. Another option is to generate a new planning target volume (PTV) by subtracting the expanded critical structure from the original PTV. The treatment plan can then be optimized using this "modified PTV" to confine the portion of the PTV receiving less than the prescription dose to the PTV-critical structure interface. By targeting the radiation beams to the edges of the "modified PTV" instead of the original PTV by applying beam collimators to the modified PTV, a sharper dose gradient can be created at the PTV-critical structure interface, allowing for better sparing of the critical structure while maintaining good dose coverage of the target volume. The collimator size chosen for beam generation is dependent on the target dimensions, complexity and location. Either the fixed or the Iris™ collimating systems can be used. However, with the fixed cones, the number of cone sizes is typically limited to three to reduce treatment time, because as mentioned previously in this chapter during treatment delivery, the robot has to traverse the treatment path with each cone separately. This limitation in the number of aperture diameters to be selected is not a concern when using the Iris™, as the robot can change apertures at a given beam position during single treatment path traversal. The smallest Iris™ apertures (i.e., 5 and 7.5 mm) are typically avoided during treatment planning as small differences in field size can result in significantly large differences in beam output [35, 36].

Once the user selects the beam apertures, a set of a few thousand-candidate beams is generated. These beams are defined based on the node positions, target location, and collimators chosen. Either isocentric targeting or conformal targeting can be chosen for planning CK brain cases. In isocentric targeting, all beams point toward a single user specified target location within the

http://dx.doi.org/10.5772/64481

tumor, and there is only one beam per node position. Isocentric planning is mostly used for simple cases, where the lesion is nearly spherical and not adjacent to critical structures. With conformal targeting, beams target multiple locations within the tumor. The target points are randomly distributed over the tumor perimeter, and multiple beams per node position are utilized. A typical plan consists of over a hundred nonisocentric, noncoplanar beams (**Figure 7b**) in the conformal targeting scenario. Conformal targeting is useful for complicated brain cases. Beam entry through the eyes is typically prohibited.

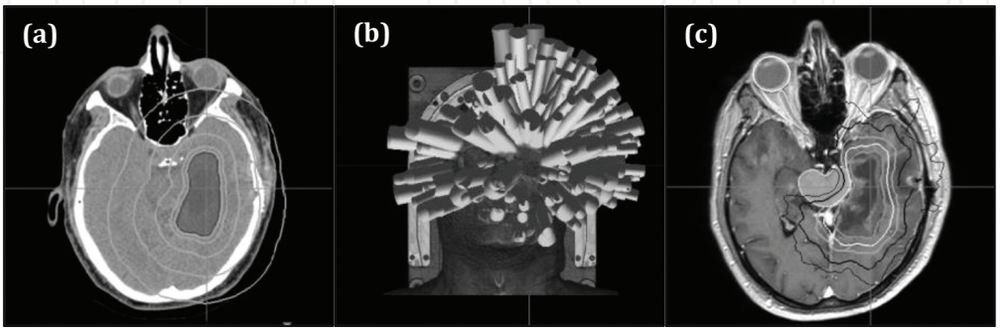

Figure 7. (a) Shell structures (a total of five shown here) generated surrounding the planning target volume to improve dose conformity and produce sharp dose gradients outside of the target. (b) A 3D representation of the beam angles used for an example CK brain treatment in which over a hundred nonisocentric, noncoplanar beams are being used. (c) Isodose distribution for an example CK brain treatment in which the planning target volume abuts the brain stem. The dose distribution is displayed on the MR images used for target delineation.

The user can also constrain the total number of monitor units (MUs) to be used for a plan, as well as specify the monitor units that should be used per node and per beam. Constraining the contribution of monitor units (MUs) from a given beam/node allows a wider distribution (or spread in beam angles) of nonisocentric, noncoplanar beams, and limits a high dose contribution from a single direction. This helps minimize "dose fingers" (high dose (typically >40–50% of the prescription dose) streaks/areas spanning from outside of the target volume toward the skin, that are shaped similar to a finger) and dose hot spots in normal tissue. The maximum MUs per node were set to be slightly higher than the maximum MUs per beam to allow for multiple beams per node. For a typical brain plan, the total MUs are ~5–10 times the prescription dose.

The dose distribution is optimized by adjusting the weighting of the beam MUs in the candidate beam set generated based on the user specified dose objectives/constraints, to minimize a linear cost function. Sequential optimization [37] is commonly used in treatment planning, where different optimization objectives such as target coverage, conformity, and dose constraints to critical structures are addressed sequentially in a user-specified order. The optimization moves from one step to the next, only when those goals set by the planner are met within user-specified relaxation criteria. This allows the user to prioritize goals (i.e., target coverage vs. critical structure sparing) in a clinically significant patient specific manner. MultiPlan™ (the CyberKnife treatment planning software) further allows for the generation of multiple shell structures of varying radii surrounding the target volume (**Figure 7a**). Dose constraints applied to these shells can be manipulated to achieve a highly conformal plan and

to guide and tighten the dose fall of outside of the target volume. In addition, beam reduction and time reduction tools are available to the planner to assess and improve plan efficiency without compromising plan quality.

The CK treatment planning system provides two dose calculation algorithms: (1) Ray-tracing and (2) Monte Carlo. Ray-tracing uses the effective path length to determine dose deposition based on tissue heterogeneities, and is based on a pencil beam approach in which a single beam is considered to constitute of many single rays [33]. However, photon scatter and lateral electron scatter in heterogeneous media are not correctly accounted for with Ray-tracking as is with Monte Carlo. This results in substantial inaccuracies in dose calculation at the interface of tissues of different densities and for those lesions that are located within low-density (i.e., lung, sinuses) and high-density (i.e., bone) tissues [38]. For example, for lung cases, using Ray-tracing for dose calculation can result in 8–11% differences compared to that calculated with Monte Carlo [38]. For brain lesions that are not adjacent to, or in, air/bone, the differences in the plans calculated using Ray-tracing compared to Monte Carlo are clinically insignificant, with the differences in maximum dose to the critical structures and tumor coverage generally found to be <5% between the two calculation methods [39]. However, for those lesions that are located in/adjacent to the sinus cavity or bony anatomy, dose calculation with Monte Carlo may provide more accurate results. The Monte Carlo algorithm uses theoretical simulation and experimental results to calculate dose deposition from each particle traveling through tissue, considering its interactions with other particles. The Monte Carlo platform specifically employed within the CK treatment planning system uses a single source model, which simulates photon interactions with media for a variety of photon energies. The travel paths of the secondary electrons generated by the interaction of photons with tissue are further considered. Dose deposition by these charged particles is calculated considering tissue density differences and electron stopping powers [38].

2.2.2. Typical treatment planning dose volume constraints

Typical fractionation schemes for CK brain treatments are 25 or 30 Gy in five fractions. Single and three fraction dose schemes are also sometimes used. Dose constraints to critical structures are mainly based on those recommend by AAPMs Task Group Report [40] as given in **Table 1**.

		Single fraction		**Three fractions**		**Five fractions**	
Serial structure	**Max critical volume above threshold**	**Threshold dose (Gy)**	**Max point dose (Gy)**	**Threshold dose (Gy)**	**Max point dose (Gy)**	**Threshold dose (Gy)**	**Max point dose (Gy)**
Optic pathway	<0.2 cc	8	10	15.3	17.4	23	25
Cochlea			9		17.1		25
Brainstem (not medulla)	<0.5 cc	10	15	18	23.1	23	31
Spinal cord and medulla	<0.35 cc	10	14	18	21.9	23	30
	<1.2 cc	7		12.3		14.5	

Table 1. Dose constraints for hypofractionated brain treatments as recommended by AAPMs Task Group 101.

http://dx.doi.org/10.5772/64481

Figure 7c shows an example of a complicated brain CK plan in which the target volume abuts the brainstem. A prescription dose of 25 Gy was prescribed to the planning target volume in five fractions in this particular case. Dose was prescribed to the 70% isodose line. The brain stem maximum dose (0.035 cc) for this particular case was kept below 22 Gy. The optic chiasm maximum dose was <9 Gy and the optic nerve maximum dose was ~10 Gy. The gradient index and the conformality index (nCI) for this particular plan was 2.92 and 1.13, respectively. The dose distribution within the target volume is highly heterogeneous as is commonly the case for CK plans, because typical prescription isodose lines for brain treatments vary between 60 and 75%. However, with the CyberKnife, the planner can guide the optimization to achieve a plan prescribing to a wide range of isodoselines. Therefore, CK plans can be tailored to achieve plans similar to Gamma Knife plans (by optimizing the plan such that the prescription isodose is ~50%) or linac based SRS/SBRT plans (by optimizing the plan such that the prescription isodose is between 70 and 80%).

2.3. Clinical studies – hypofractionated brain treatments

Several clinical investigations have reported on the safety and efficacy of hypofractionated CK brain treatments. One such study [41] looking at CK treatments for large brain metastases delivering 30–41 Gy in 3–5 fractions, reported a crude local tumor control (LTC) rate of 86.8%. The estimated LTC rates at 12 and 24 months were 87 and 65.2%. The median overall survival and progression-free survival rates were 16 and 11 months, respectively. Patient performance status and preoperative neurologic deficits reportedly improved in 57.1 and 70.6%, respectively. Another study [42] evaluating the efficacy and toxicity of 5-fraction CK radiotherapy in patients with large brain metastases in critical areas, demonstrated that a high rate of local tumor control and low rate of complications are achievable. They report a local tumor control rate of 92.9% during a median follow-up of 8 months and report that neurological manifestations improved in 50.9% of the patients.

2.4. Intrafractional monitoring and treatment delivery

A 6D Skull Tracking is the tracking method used for CK brain treatments. This method is frameless and uses the bony anatomy of the skull obtained from 2D X-ray imaging for patient set up and for determining and correcting for patient motion during treatment delivery. This tracking method can be used for intracranial, head and neck, and certain upper spine (C1, C2) treatments. The algorithm assumes a fixed relationship, between the target, the "align center" and the bony anatomy of the skull. The "align center" (also referred to as the imaging center) is user defined during treatment planning. For brain treatments, the "align center" is chosen such that the superior and anterior parts of the skull are ~10–15 mm from the edge of the imaging field-of-view (**Figure 8**).

Prior to treatment start, the patient is immobilized and positioned as during simulation. Patient setup is carried out through a motorized couch, which has either 5 (standard couch) or 6 (RoboCouch™) degrees of freedom. A pair of X-ray images is taken to make gross adjustments to the patient position, which can then be fine-tuned using automatic couch movements. Correct positioning is confirmed by comparing the live X-ray images to DRRs from the

treatment planning CT. The algorithm correlates the live X-ray images with the DRRs based on pixel similarity criteria. X-ray technique (kV, mAs and exposure time) needs to be optimized by using parameters provided by the software showing differences in the estimated align center position based on each image along the common superior/inferior axis, similarity of overall image intensity between the live images and the DRRs, and the presence of external objects in the X-ray image that are not on the DRR.

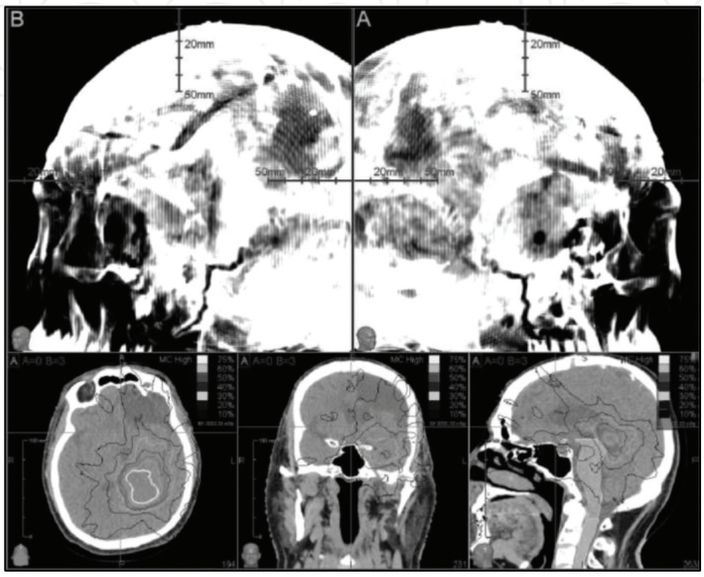

Figure 8. An example of how the "align center" or the imaging center is specified during treatment planning for an example CK brain treatment. The "align center" is chosen such that the superior and anterior parts of the skull on the DRRs are ~10–15 mm from the edge of the imaging field-of-view. The bottom portion displays the placement of the cross hairs on the planning CT images to achieve the appropriate placement of the skull on the DRR images as shown on the top panel.

Once the beam is on for treatment, orthogonal X-rays are intermittently taken (at time intervals of 30–60 sec (lower imaging interval can be chosen on a case-by-case basis). These images are automatically registered to the DRRs derived from the treatment planning CT. Unique to the CKS, the robotic manipulator uses this near real-time target position information to retarget the radiation beam to the current target position, thus eliminating the need for patient repositioning. The robot can automatically correct for translations up to 10 mm, and rotations of 1, 1, and 3° for the roll, yaw and pitch, respectively.

Submillimeter accuracy is achievable through 6D Skull Tracking. A recent study [43] used log files generated by the CKS, as well as the actual treatment parameters from each procedure to investigate the mechanical uncertainty in beam localization over a time period of approximately 1 year. They further evaluated patterns of patient movement during brain CK treatments. They found the mean mechanical uncertainties of CK brain tumor treatments to be 0.07, 0.01, and −0.09 mm in the +inferior/−superior, +left/−right, and +anterior/−posterior directions, respectively and conclude the CK to be robust in tracking accuracy regardless of patient's movement. Their investigations further found a CTV-PTV margin of 2.0 mm to be adequate in brain tumor treatments for an on-treatment imaging interval of 30–45 sec.

http://dx.doi.org/10.5772/64481

2.5. Future developments

As mentioned earlier in the chapter, a new CK system equipped with three interchangeable collimating systems (fixed, Iris, and MLC) is now available for clinical use. This new CK M6 platform has the potential to improve the efficiency of hypofractionated CK treatments and to further extend the advantages of noncoplanar treatment and real-time tracking to conventionally fractionated treatment. A recent study [44] assessing the clinical capabilities of the CK-MLC for hypofractionated brain SBRT demonstrated that treatment plans generated with the CK-MLC were of equal or better quality compared to clinically approved CK plans using circular (fixed/Iris™) collimators. The total monitor units were reduced by 70%, and the treatment time could be reduced by nearly a half by using the CK-MLC, with an average treatment time of 17 min compared to 30 min for plans using circular apertures.

3. Hypofractionated S-Band linac-based radiosurgery

In the 1986, Lutz and Winston described "A small field irradiation technique to deliver high doses of single fraction photon radiation to small, precisely located volumes (0.5–8 cm^3) within the brain". This marked the beginning of brain SRS with linear accelerators [45, 46]. Now 30 years later, the clinicians have a new generation of radiation therapy machines, which are designed from the ground up to combine the fast delivery of high dose rate from flattening filter free (FFF) beam and precise tumor localization with image guided radiotherapy (IGRT), at their service to push the boundary of SRS with escalated dose protocols and innovative fraction scheme, limiting side effects and sparing nearby organs at risk. **Figure 9** shows the two modern linear accelerators from Varian (left panel) and Elekta (right panel), respectively.

Figure 9. Two state-of-the-art medical linear accelerators that are capability of high-precision hypofractionated treatments: left panel shows Edge manufactured from Varian Oncology (Palo Alto, CA) and right panel shows Versa HD manufactured from Elekta Company (Atlanta, GA).

The newest generation of Linac from Varian, Edge, has X-ray output energies at 6MV (600 MU/min), 6X FFF mode (1400 MU/min) and 10X FFF mode (2400 MU/min). With gantry and collimator isocenters accuracy smaller than 0.5 mm radius, gantry, collimator, and couch

isocenters accuracy smaller than 0.75 mm radius and gantry rotational accuracy smaller than 0.3°, the Edge has the mechanical performance required for SRS. The high definition 120 leaf MLC, moving at a maximum speed of 2.5 cm/sec, with an extra fine MLC leaf at 2.5 mm in the central 20 cm and 40 × 22 cm field size, can treat most of the smaller brain tumors.

Versa HD, the latest offering from Elekta, can treat patient with 6 MV-15 MV at 600 MU/min, 6× FFF mode at 1400 MU/min and 10× FFF mode at 2200 MU/min. It also carries the Agility MLC with 80 MLC pairs at 5 mm width across the full 40 × 40 cm field and a speed up to 3.5 cm/sec. When coupled with dynamic leaf guide, the MLC leaf move at an effective speed of 6.5 cm/sec. Gantry, collimator, and couch isocentricity measurements were within 1, 0.7, and 0.7 mm diameter, respectively [47].

3.1. Beam and patient positioning characteristics

3.1.1. Fast delivery with FFF beam and VMAT

The major drawback of performing SRS with a conventional linear accelerator is the long delivery time results from the low dose rate. For hypofractionated SRS with 2000 MU per fraction, the beam on time alone is ~3 min for conventional beams. In 1991, O'Brien PF presented in his paper that after removed the flattening filter from an AECL Therac-6 linear accelerator, the dose rate is increased by a factor of 2.75. Now almost all major linacs can operate in the FFF mode with maximum dose at ~2400 MU/min. Volumetric-modulated arc therapy, a rotational arc therapy with intensity modulation, achieves highly conformal dose distributions with great treatment delivery efficiency and reduced total MU. The VMAT delivery, in conjunction with the FFF mode, can lead to even greater efficiency in delivery. One study [48] compared VMAT FFF plan with IMRT flat beams and found that the mean beam-on time difference was 6.79 min (74.9% decrease); mean treatment delivery time difference was 8.99 min (range: 5.40–13.05 min), a relative improvement of 71.1% (range: 53.4–82.4%) for plans with high dose fractionations (16–20 Gy/fraction).

3.1.2. Patient positioning with frameless system

With the introduction of on board KV MV imaging and the development of image guided radiotherapy, frameless intracranial systems become an alternative to the invasive frames used traditionally to establish the stereotactic coordinates of the targets and ensure the accuracy of immobilization and positioning such as the Leksell stereotactic frame. The frameless SRS brings patient convenience and comfort, enables an efficient workflow for hypofractionation, and makes SRS more available where there is no neurosurgical support. **Figure 10** shows the Leksell frame, Brainlab frameless mask, and Civco's trUpoint Arch system.

The patient immobilization is ensured by the bite-block and thermoplastic masks. The six optical marking spheres on top of the Brainlab mask monitored by infrared camera on roof provide real-time tracking of the departure from the treatment isocenter and information to determine X-ray imaging frequency. One study has compared four frameless, thermoplastic mask-based immobilization strategies for inter- and intrafraction patient positioning uncer-

http://dx.doi.org/10.5772/64481

tainties [49]. They studied four systems including: (1) head mask with head cushion; (2) head mask with head cushion and a body immobilizer; (3) head mask and cushion with shoulder mask and cushion; and (4) same as (3) plus a mouthpiece. The system (4) has a mean interfraction translational shift of 2.1 (±1.0) mm and intrafraction motion of 0.7 (±0.8) mm, providing the best accuracy and stability overall.

Figure 10. Left: Leksell frame; middle: Brainlab localization array mask; and right: CIVCO mask.

3.2. Imaging guidance

3.2.1. In-room KV/MV imaging

The comparison of the portal images from electronic portal imaging devices (EPID) with DRR is the most commonly used patient positioning verification, which can be performed with either KV on board imager providing higher soft tissue contrast or MV imaging with the treatment beam when bones or fiducial marks can be used for alignment. Usually an orthogonal image pair is acquired and followed by the automatic shift calculation with the computer and appropriate correction by the treatment couch. For an improvement of the target visualization, CBCT can also be performed. As a complementary to the on-linac imaging mainly for patient initial setup, several commercial product provide intrafraction continuous monitoring of the patient's position. The Exac-trac X-ray system consists of two oblique X-ray imagers, with two floor mounted KV X-ray tubes and two corresponding flat panel detectors on the ceiling (**Figure 11**). The system can take images at any gantry or couch angle. With the 6D fusion option, the system can calculate patient's position variation in three translational direction and three rotational directions. Another system to monitor intrafraction movement is through monitoring patient's surface features such as the AlignRt system, where a high-resolution 3D-rendered surface of the patient from the pseudo-random pattern projected on the patient's skin, using stereo vision techniques and a triangulation process without any ionization radiation.

3.2.2. Six degrees-of-freedom couch

With all the advancements of the field of IGRT, a further improvement of patient setup can be achieved by the new generation of six degrees-of-freedom (6DoF) couch that can correct the

patient setup in three translational axes and three rotation axes. One group of investigators performed tests to request a known shift for the 6DoF couch and compared this requested shift with the actually applied shift by independently measuring the applied shift using different methods (graph paper, laser, inclinometer, and imaging system) [50]. The study found that the deviations were −0.01 ± 0.02, 0.01 ± 0.02, and 0.01 ± 0.02 cm for the longitudinal, lateral, and vertical axes, respectively; 0.03 ± 0.06, −0.04 ± 0.12, and −0.01 ± 0.08° for the three rotational axes couch rotation, pitch, and roll, respectively.

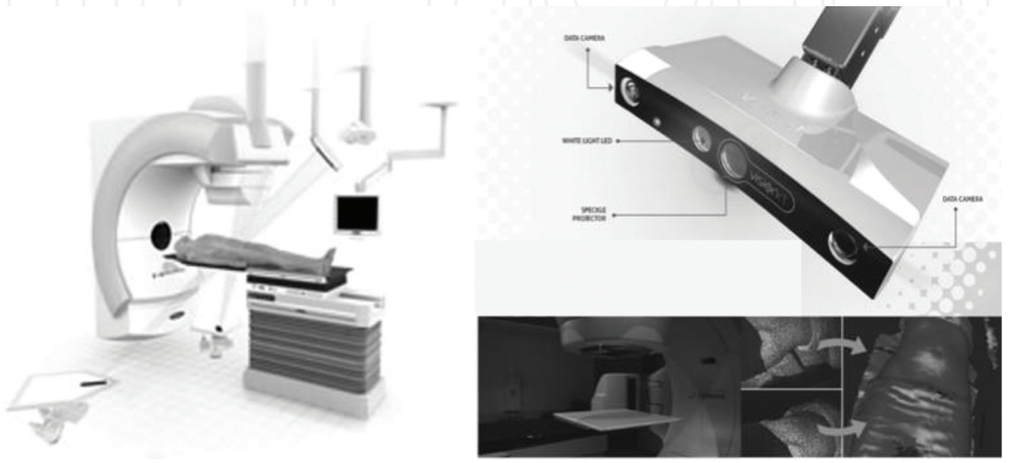

Figure 11. Left panel: Exactrac X-ray imaging system (Novalis) and right panel: surface-based patient alignment system (AlignRt).

The combination of in-room imaging and robotic couch can achieve high precision in cranial treatment of immobilized patients. One European group has demonstrated translational repositioning accuracy of 0.9 ± 0.5 mm for 47 consecutive patients with 372 fractions [51].

3.3. Treatment planning

3.3.1. Cone-based planning

By using cone collimators and multiple intersecting noncoplanar arcs, the linac can deliver dose distribution similar to that of the Gamma Knife. It produced a tight spherically shaped high dose region with sharp dose fall-off (**Figure 12**).

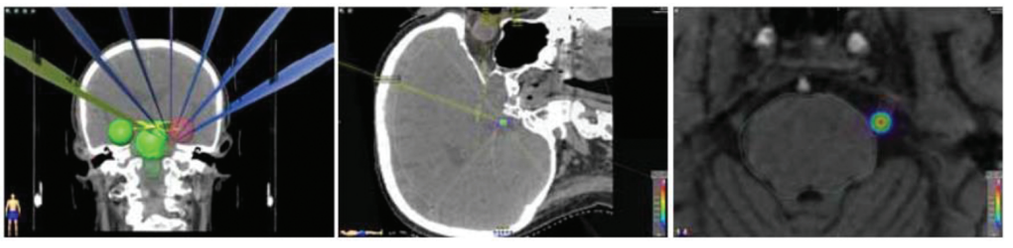

Figure 12. Illustration of a treatment plan case on the Brainlab system.

http://dx.doi.org/10.5772/64481

3.3.2. VMAT

VMAT offers shorter treatment times that are consistent with the goals of IGRT. It facilitates sparing proximal normal tissues compared to the fixed aperture techniques and simultaneously treating multiple targets with a single isocenter. One group showed that SRS using VMAT is a viable alternative to other techniques and enables short treatment times [52]. Another group replanned older model Gamma Knife (GK Model C) treatments of multiple cranial metastases with multi-arc (MA) and single-arc (SA), single-isocenter VMAT (RapidArc) in Eclipse [22]. They found that for multiple target SRS, 4-arc VMAT produced clinically equivalent conformity, dose fall-off, 12 Gy isodose volume, and low isodose spill, and reduced treatment time compared to an early GK Model C.

4. Summary

In this chapter, we have systematically highlighted three state-of-the-art hypofractionated SRS modalities in intracranial applications. With rapid maturing in technology and growing integration of hardware and software in the realm of hypofractionated brain SRS, clinical applications and consensus guidelines are emerging. Both international and national regional societies such as the international stereotactic radiosurgery society (ISRS) and American Association of Physicists in Medicine (AAPM) have initiated joint effort toward developing clinical practice and consensus guidelines. From the physical point of view, future trends in the field will continue to move toward significant enhancements in the areas of (1) imaging guidance, (2) online treatment adaption, and (3) biological tissue effect quantifications for hypofractionated radiosurgery of large and/or complex brain lesions.

Author details

Dilini Pinnaduwage[1], Peng Dong[2] and Lijun Ma[3*]

*Address all correspondence to: lijun.ma@ucsf.edu

1 Department of Radiation Oncology, The University of Arizona School of Medicine/St. Joseph's Hospital Medical Center, Phoenix, AZ, USA

2 Department of Radiation Oncology, Stanford University, Stanford, CA, USA

3 Department of Radiation Oncology, University of California San Francisco, San Francisco, CA, USA

References

[1] Leksell L. 1951. The stereotaxic method and radiosurgery of the brain. *Acta Chir Scand* 102: 316–9.

[2] Wu A, Lindner G, Maitz A H, Kalend A M, Lunsford L D, Flickinger J C and Bloomer W D. 1990. Physics of Gamma Knife approach on convergent beams in stereotactic radiosurgery. *Int J Radiat Oncol Biol Phys* 18: 941–9.

[3] Andrews D W, Bednarz G, Evans J J and Downes B. 2006. A review of 3 current radiosurgery systems. *Surg Neurol* 66: 559–64.

[4] Kano H, Sheehan J, Sneed P K, McBride H L, Young B, Duma C, Mathieu D, Seymour Z, McDermott M W, Kondziolka D, Iyer A and Lunsford L D. 2015. Skull base chondrosarcoma radiosurgery: report of the North American Gamma Knife Consortium. *J Neurosurg* 123: 1268–75.

[5] Regis J, Tuleasca C, Resseguier N, Carron R, Donnet A, Gaudart J and Levivier M. 2016. Long-term safety and efficacy of Gamma Knife surgery in classical trigeminal neuralgia: a 497-patient historical cohort study. *J Neurosurg* 124: 1079–87.

[6] Sahgal A, Ma L, Chang E, Shiu A, Larson D A, Laperriere N, Yin F F, Tsao M, Menard C, Basran P S, Letourneau D, Heydarian M, Beachey D, Shukla V, Cusimano M, Hodaie M, Zadeh G, Bernstein M and Schwartz M. 2009. Advances in technology for intracranial stereotactic radiosurgery. *Technol Cancer Res Treat* 8: 271–80.

[7] Sheehan J P, Kano H, Xu Z, Chiang V, Mathieu D, Chao S, Akpinar B, Lee J Y, Yu J B, Hess J, Wu H M, Chung W Y, Pierce J, Missios S, Kondziolka D, Alonso-Basanta M, Barnett G H and Lunsford L D. 2015a. Gamma Knife radiosurgery for facial nerve schwannomas: a multicenter study. *J Neurosurg* 123: 387–94.

[8] Sheehan J P, Starke R M, Kano H, Barnett G H, Mathieu D, Chiang V, Yu J B, Hess J, McBride H L, Honea N, Nakaji P, Lee J Y, Rahmathulla G, Evanoff W A, Alonso-Basanta M and Lunsford L D. 2015b. Gamma Knife radiosurgery for posterior fossa meningiomas: a multicenter study. *J Neurosurg* 122: 1479–89.

[9] Snell M, Bova F, Larson D, Leavitt D, Lutz W, Podgorsak E and Wu A. 1995. *Stereotactic Radiosurgery, Report of TG42.* Wisconsin: Medical Physics Publishing.

[10] Grandhi R, Kondziolka D, Panczykowski D, Monaco E A, 3rd, Kano H, Niranjan A, Flickinger J C and Lunsford L D. 2012. Stereotactic radiosurgery using the Leksell Gamma Knife Perfexion unit in the management of patients with 10 or more brain metastases. *J Neurosurg* 117: 237–45.

[11] Lindquist C and Paddick I. 2007. The Leksell Gamma Knife Perfexion and comparisons with its predecessors. *Neurosurgery* 61: 130–40; discussion 40-1.

[12] Ma L, Verhey L, Chuang C, Descovich M, Smith V, Huang K, McDermott M and Sneed P. 2008. Effect of composite sector collimation on average dose fall-off for Gamma Knife Perfexion. *J Neurosurg* 109(Suppl): 15–20.

[13] Regis J, Tamura M, Guillot C, Yomo S, Muraciolle X, Nagaje M, Arka Y and Porcheron D. 2009. Radiosurgery with the world's first fully robotized Leksell Gamma Knife PerfeXion in clinical use: a 200-patient prospective, randomized, controlled comparison with the Gamma Knife 4C. *Neurosurgery* 64: 346–55; discussion 55-6.

[14] Al-Omair A, Soliman H, Xu W, Karotki A, Mainprize T, Phan N, Das S, Keith J, Yeung R, Perry J, Tsao M and Sahgal A. 2013. Hypofractionated stereotactic radiotherapy in five daily fractions for post-operative surgical cavities in brain metastases patients with and without prior whole brain radiation. *Technol Cancer Res Treat. **12**(6): 493–499*

[15] Devriendt D, De Smedt F, Glineur R and Massager N. 2015. Five-fraction Gamma Knife radiosurgery using the extend relocatable system for benign neoplasms close to optic pathways. *Pract Radiat Oncol* 5: e119–25.

[16] Ma L, Pinnaduwage D, McDermott M and Sneed P K. 2014c. Whole-procedural radiological accuracy for delivering multi-session Gamma Knife radiosurgery with a relocatable frame system. *Technol Cancer Res Treat* 13: 403–8.

[17] Schlesinger D, Xu Z, Taylor F, Yen C P and Sheehan J. 2012. Interfraction and intrafraction performance of the Gamma Knife extend system for patient positioning and immobilization. *J Neurosurg* 117(Suppl): 217–24.

[18] Ma L, Chiu J, Hoye J, McGuiness C and Perez-Andujar A. 2014a. Quality assurance of stereotactic alignment and patient positioning mechanical accuracy for robotized Gamma Knife radiosurgery. *Phys Med Biol* 59: N221–6.

[19] Paddick I. 2000. A simple scoring ratio to index the conformity of radiosurgical treatment plans. Technical note. *J Neurosurg* 93(Suppl. 3): 219–22.

[20] Paddick I and Lippitz B. 2006. A simple dose gradient measurement tool to complement the conformity index. *J Neurosurg* 105(Suppl): 194–201.

[21] Ma L, Sahgal A, Descovich M, Cho Y B, Chuang C, Huang K, Laperriere N J, Shrieve D C and Larson D A. 2010. Equivalence in dose fall-off for isocentric and nonisocentric intracranial treatment modalities and its impact on dose fractionation schemes. *I J Radiat Oncol, Biol, Phys* 76: 943–8.

[22] Thomas E M, Popple R A, Wu X, Clark G M, Markert J M, Guthrie B L, Yuan Y, Dobelbower M C, Spencer S A and Fiveash J B. 2014. Comparison of plan quality and delivery time between volumetric arc therapy (RapidArc) and Gamma Knife radiosurgery for multiple cranial metastases. *Neurosurgery* 75: 409–17; discussion 17-8.

[23] Ma L, Nichol A, Hossain S, Wang B, Petti P, Vellani R, Higby C, Ahmad S, Barani I, Shrieve D C, Larson D A and Sahgal A. 2014b. Variable dose interplay effects across

radiosurgical apparatus in treating multiple brain metastases. *Int J Comput Assist Radiol Surg.* 9(6): 1079–86

[24] Ma L, Petti P, Wang B, Descovich M, Chuang C, Barani I J, Kunwar S, Shrieve D C, Sahgal A and Larson D A. 2011. Apparatus dependence of normal brain tissue dose in stereotactic radiosurgery for multiple brain metastases. *J Neurosurg* 114: 1580–4.

[25] Ma L, Xia P, Verhey L J and Boyer A L. 1999. A dosimetric comparison of fan-beam intensity modulated radiotherapy with Gamma Knife stereotactic radiosurgery for treating intermediate intracranial lesions. *Int J Radiat Oncol Biol Phys* 45: 1325–30.

[26] Luan S, Swanson N, Chen Z and Ma L. 2009. Dynamic Gamma Knife radiosurgery. *Phys Med Biol* 54: 1579–91.

[27] Ma L, Mason E, Sneed P K, McDermott M, Polishchuk A, Larson D A and Sahgal A. 2015. Clinical realization of sector beam intensity modulation for Gamma Knife radiosurgery: a pilot treatment planning study. *Int J Radiat Oncol Biol Phys* 91: 661–8.

[28] Adler JR.(1993) Frameless Radiosurgery. In Stereotactic Surgery and Radiosurgery, ed. AAF De Salles and SJ Goetsch, 237–48. Madison: Medical Physics Publishing.

[29] Adler JR, Cox RS. 1996. *Preliminary Experience with CyberKnife – Radiosurgery*. Basel: S. Karger; pp. 112–38.

[30] Kilby W, Dooley J R, Kuduvalli G, Sayeh S and Maurer C R, Jr. 2010. The CyberKnife robotic radiosurgery system in 2010. *Technol Cancer Res Treat* 9: 433–52.

[31] Echner G G, Kilby W, Lee M, Earnst E, Sayeh S, Schlaefer A, Rhein B, Dooley J R, Lang C, Blanck O, Lessard E, Maurer C R, Jr. and Schlegel W. 2009. The design, physical properties and clinical utility of an iris collimator for robotic radiosurgery. *Phys Med Biol* 54: 5359–80.

[32] Accuray Inc. 2013 *CyberKnife M6 Series Technical Specifications.* Madison, WI: Accuray.

[33] Pinnaduwage DS, Descovich M and Ma L. 2014. Treatment planning, intrafractional tracking and delivery: CyberKnife-based stereotactic body radiation therapy. *Stereotactic Body Radiat Therapy Spinal Metastasis*, ed. SL Simon, A Sahgal, BS The, PC Gerszten and EL Chang, 57–75. UK: Future Science Group.

[34] Adler J R, Jr., Murphy M J, Chang S D and Hancock S L. 1999. Image-guided robotic radiosurgery. *Neurosurgery* 44: 1299–306; discussion 306-7.

[35] Francescon P, Kilby W, Satariano N and Cora S. 2012. Monte Carlo simulated correction factors for machine specific reference field dose calibration and output factor measurement using fixed and iris collimators on the CyberKnife system. *Phys Med Biol* 57: 3741–58.

[36] Pantelis E, Moutsatsos A, Zourari K, Petrokokkinos L, Sakelliou L, Kilby W, Antypas C, Papagiannis P, Karaiskos P, Georgiou E and Seimenis I. 2012. On the output factor measurements of the CyberKnife iris collimator small fields: experimental determina-

tion of the k(Q(clin),Q(msr)) (f(clin),f(msr)) correction factors for microchamber and diode detectors. *Med Phys* 39: 4875–85.

[37] Schlaefer A and Schweikard A. 2008. Stepwise multi-criteria optimization for robotic radiosurgery. *Med Phys* 35: 2094–103.

[38] Wilcox E E, Daskalov G M, Lincoln H, Shumway R C, Kaplan B M and Colasanto J M. 2010. Comparison of planned dose distributions calculated by Monte Carlo and Ray-Trace algorithms for the treatment of lung tumors with cyberknife: a preliminary study in 33 patients. *Int J Radiat Oncol Biol Phys* 77: 277–84.

[39] Wilcox E E, Daskalov G M and Lincoln H. 2011. Stereotactic radiosurgery-radiotherapy: Should Monte Carlo treatment planning be used for all sites? *Pract Radiat Oncol* 1: 251–60.

[40] Benedict S H, Yenice K M, Followill D, Galvin J M, Hinson W, Kavanagh B, Keall P, Lovelock M, Meeks S, Papiez L, Purdie T, Sadagopan R, Schell M C, Salter B, Schlesinger D J, Shiu A S, Solberg T, Song D Y, Stieber V, Timmerman R, Tome W A, Verellen D, Wang L and Yin F F. 2010. Stereotactic body radiation therapy: the report of AAPM Task Group 101. *Med Phys* 37: 4078–101.

[41] Jeong W J, Park J H, Lee E J, Kim J H, Kim C J and Cho Y H. 2015. Efficacy and safety of fractionated stereotactic radiosurgery for large brain metastases. *J Korean Neurosurg Soc* 58: 217–24.

[42] Inoue H K, Sato H, Seto K, Torikai K, Suzuki Y, Saitoh J, Noda S E and Nakano T. 2014. Five-fraction CyberKnife radiotherapy for large brain metastases in critical areas: impact on the surrounding brain volumes circumscribed with a single dose equivalent of 14 Gy (V14) to avoid radiation necrosis. *J Radiat Res* 55: 334–42.

[43] Okamoto H, Hamada M, Sakamoto, Wakita A, Nakamura S, Kato T, Abe Y, Takahashi K, Igaki H and Itami J. 2016. Log-file analysis of accuracy of beam localization for brain tumor treatment by CyberKnife. *Prac Radiat Oncol* In press.

[44] McGuinness C M, Gottschalk A R, Lessard E, Nakamura J L, Pinnaduwage D, Pouliot J, Sims C and Descovich M. 2015. Investigating the clinical advantages of a robotic linac equipped with a multileaf collimator in the treatment of brain and prostate cancer patients. *J Appl Clin Med Phys* 16: 5502.

[45] Lutz W, Winston K R and Maleki N. 1988. A system for stereotactic radiosurgery with a linear accelerator. *Int J Radiat Oncol Biol Phys* 14: 373–81.

[46] Winston K R and Lutz W. 1988. Linear accelerator as a neurosurgical tool for stereotactic radiosurgery. *Neurosurgery* 22: 454–64.

[47] Narayanasamy G, Saenz D, Cruz W, Ha C S, Papanikolaou N and Stathakis S. 2016. Commissioning an Elekta Versa HD linear accelerator. *J Appl Clin Med Phys* 17: 5799.

[48] Thomas E M, Popple R A, Prendergast B M, Clark G M, Dobelbower M C and Fiveash J B. 2013. Effects of flattening filter-free and volumetric-modulated arc therapy delivery on treatment efficiency. *J Appl Clin Med Phys* 14: 4328.

[49] Tryggestad E, Christian M, Ford E, Kut C, Le Y, Sanguineti G, Song D Y and Kleinberg L. 2011. Inter- and intrafraction patient positioning uncertainties for intracranial radiotherapy: a study of four frameless, thermoplastic mask-based immobilization strategies using daily cone-beam CT. *Int J Radiat Oncol Biol Phys* 80: 281–90.

[50] Schmidhalter D, Fix M K, Wyss M, Schaer N, Munro P, Scheib S, Kunz P and Manser P. 2013. Evaluation of a new six degrees of freedom couch for radiation therapy. *Med Phys* 40: 111710.

[51] Guckenberger M, Meyer J, Wilbert J, Baier K, Sauer O and Flentje M. 2007. Precision of image-guided radiotherapy (IGRT) in six degrees of freedom and limitations in clinical practice. *Strahlenther Onkol* 183: 307–13.

[52] Mayo C S, Ding L, Addesa A, Kadish S, Fitzgerald T J and Moser R. 2010. Initial experience with volumetric IMRT (RapidArc) for intracranial stereotactic radiosurgery. *Int J Radiat Oncol Biol Phys* 78: 1457–66.